
A BDDC PRECONDITIONER FOR THE CARDIAC EMI MODEL IN THREE DIMENSIONS

A PREPRINT

Fritz Göbel^{1,*}, Ngoc Mai Monica Huynh², Fatemeh Chegini³, Luca Franco Pavarino², Martin Weiser³, Simone Scacchi⁴, and Hartwig Anzt¹

¹School of Computation, Information and Technology, Technical University of Munich, Bildungscampus 2, 74076 Heilbronn, Germany.

²Dipartimento di Matematica, Università degli Studi di Pavia, Via Ferrata, 27100 Pavia, Italy.

³Zuse Institute Berlin, Takustraße 7, 14195 Berlin, Germany.

⁴Dipartimento di Matematica, Università degli Studi di Milano, Via Saldini 50, 20133 Milano, Italy.

*Corresponding author: Fritz Göbel, fritz.goebel@tum.de

14/02/2025

1 Introduction

This work aims at generalizing a previous convergence analysis of BDDC preconditioners for cardiac cell-by-cell models [16] to three spatial dimensions. Such models on the microscopic level have been studied over the past years in order to understand events in aging and structurally diseased hearts which macroscopic Monodomain and Bidomain models [21, 24, 28] that are based on a homogenized description of the cardiac tissue fail to adequately represent. In such events, reduced electrical coupling leads to large differences in behavior between neighboring cells, which requires careful modeling of each individual cardiac cell.

We consider the EMI (Extracellular space, cell Membrane and Intracellular space) model, which has been introduced and analyzed in [6, 15, 18, 19, 25, 26] and has been at the core of the EuroHPC project MICROCARD [1]. Throughout the course of this project, Balancing Domain Decomposition by Constraints (BDDC) preconditioners (we refer to [20, 23] for extensive explanations of such algorithms) have been identified to be an efficient choice for composite Discontinuous Galerkin (DG) type discretizations of cardiac cell-by-cell models and a theoretical analysis of this method has been presented in [16], while a preliminary study on its integration with time-stepping methods can be found in [9]. Here, a key step was the careful construction of extended dual and primal spaces for the degrees of freedom, allowing for continuous mapping in the BDDC splitting while still honoring the discontinuities across cell boundaries as they occur in the EMI model. Up to now, the theoretical analysis in three dimensions remains an open question, as the introduction of edge terms into the primal space requires additional constraints. In this work, we leverage results from [14] as well as standard sub-structuring theory arguments from [23] in order to close this gap. Other paths for the solution of EMI models have been investigated, ranging from boundary element methods [10] as discretization choice, to multigrd solvers [8], overlapping Schwarz preconditioners [17] and other iterative solvers build upon ad-hoc spectral analysis [7]. Other approaches to domain decomposition preconditioning for DG type problems have been studied e.g. in [3] and [5].

For the sake of completeness, we will first give an overview of a simplified EMI model and its time and space discretizations in Section 2, referring to [19, 25, 26] for details on the EMI model and to [16] for the derivation of the time and space composite-DG discretizations. We introduce the finite element spaces, describe the BDDC preconditioner for this application, and recall the Lemmas from literature necessary to prove its convergence in Section 3 before providing a convergence proof, the main contribution of this paper, in Section 4. Finally, Section 5 presents a numerical study supporting the derived theory with practical results.

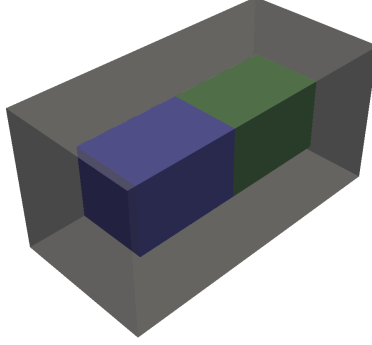


Figure 1: Visualization of two cells Ω_1 (green) and Ω_2 (blue) floating in extracellular liquid Ω_0 (grey). For this three-dimensional example, we have to consider interface terms for ionic currents between extracellular space and the cells over $F_{01} = \partial\Omega_0 \cap \partial\Omega_1$ and $F_{02} = \partial\Omega_0 \cap \partial\Omega_2$ and ionic currents through gap junctions between the cells over $F_{12} = \partial\Omega_1 \cap \partial\Omega_2$. For the BDDC preconditioner, it is important to also consider edge terms on $E_{0,\{1,2\}} = \partial\Omega_0 \cap \partial\Omega_1 \cap \partial\Omega_2$.

2 The EMI model

As in [16], we consider N myocytes immersed in extracellular liquid, together forming the cardiac tissue Ω while focusing on the case that $\Omega \subset \mathbb{R}^3$. We assign the extracellular subdomain to be Ω_0 and each of the N cardiac cells to be separate subdomains $\Omega_1, \dots, \Omega_N$, interacting with the surrounding extracellular space through ionic currents and with their neighboring myocytes via gap junctions, which are special protein channels allowing for the passage of ions directly between two cells [22]. We assume a partition of the cardiac tissue Ω into $N + 1$ non-overlapping subdomains Ω_i such that $\bar{\Omega} = \cup_{i=0}^N \bar{\Omega}_i$, $\Omega_i \cap \Omega_j = \emptyset$ if $i \neq j$.

The EMI model is described by the equations

$$\begin{cases} -\operatorname{div}(\sigma_i \nabla u_i) = 0 & \text{in } \Omega_i, i = 0, \dots, N \\ -n_i^T \sigma_i \nabla u_i = C_m \frac{\partial v_{ij}}{\partial t} + F(v_{ij}, c, w) & \text{on } F_{ij} = \partial\Omega_i \cap \partial\Omega_j, i \neq j \\ n^T \sigma_i \nabla u_i = 0 & \text{on } \partial\Omega_i \cap \partial\Omega \\ \frac{\partial c}{\partial t} - C(v_{ij}, w, c) = 0, \quad \frac{\partial w}{\partial t} - R(v_{ij}, w) = 0 & \end{cases} \quad (1)$$

with conductivity coefficients σ_i in Ω_i , outward normals n_i on $\partial\Omega_i$ and membrane capacitance for unit area C_m on the membrane surface. $v_{ij} = u_i - u_j$ describes the transmembrane voltage, i.e. the discontinuities of the electric potentials between neighboring subdomains and $F(v_{ij}, c, w)$ stands for either ionic current $I_{\text{ion}}(v_{ij}, c, w)$ or gap junction current $G(v_{ij})$, depending on whether the two neighbors are both cells or one is the extracellular domain. We assume $G(v)$ to be linear in the potential jumps v and note that generally, $F(v_{ij}, c, w) = -F(v_{ji}, c, w)$. The last two terms model the ion flow with ordinary differential equations describing the time evolution of ion concentrations c and gating variables w . More details on derivation and analysis of the EMI model can be found in [19, 25, 27].

We note that since the solution of (1) is only unique up to a constant, we require a zero average on the extracellular solution u_0 . Additionally, we mention that we consider a splitting strategy in time for the solution of (1), first solving the ionic model with jumps v_{ij} known from the previous time step and then updating the model with the solutions c and w and solving it for the electric potential. For brevity, we will from now on write $F(v_{ij}) := F(v_{ij}, c, w)$, omitting c and w .

2.1 Weak Formulation

On each subdomain Ω_i , integrating the first equations in (1) by parts and substituting in the second equation on the cell membrane, the i -th sub-problem reads: find $u_i \in H^1(\Omega_i)$ such that for all $\phi_i \in H^1(\Omega_i)$ the following holds:

$$\begin{aligned} 0 &= - \int_{\Omega_i} \operatorname{div}(\sigma_i \nabla u_i) \phi_i dx \\ &= \int_{\Omega_i} \sigma_i \nabla u_i \nabla \phi_i dx - \int_{\partial\Omega_i} n_i^T \sigma_i \nabla u_i \phi_i ds \\ &= \int_{\Omega_i} \sigma_i \nabla u_i \nabla \phi_i dx + \sum_{i \neq j} \int_{F_{ij}} (C_m \frac{\partial v_{ij}}{\partial t} + F(v_{ij})) \phi_i ds. \end{aligned}$$

Summing up the contributions of all subdomains, we get the global problem

$$\sum_{i=0}^N \int_{\Omega_i} \sigma_i \nabla u_i \nabla \phi_i dx + \frac{1}{2} \sum_{i=0}^N \sum_{j \neq i} \int_{F_{ij}} (C_m \frac{\partial [u]_{ij}}{\partial t} + F([u]_{ij})) [\phi]_{ij} ds = 0,$$

where $[u]_{ij} = u_i - u_j$ denotes the jump in value of the electric potential u_i and its neighboring u_j from the subdomain Ω_j along the boundary face $F_{ij} \subset \partial\Omega_i$.

2.2 Space and Time Discretization

Let $V_i(\bar{\Omega}_i)$ be the regular finite element space of piece-wise linear functions in $\bar{\Omega}_i$ and define the global finite element space as $V(\Omega) := V_0(\bar{\Omega}_0) \times \cdots \times V_N(\bar{\Omega}_N)$. Similar as in [14] we denote:

- The **subdomain face** shared between subdomains Ω_i and Ω_j is symbolized by $\bar{F}_{ij} := \partial\Omega_i \cap \partial\Omega_j$. We note that geometrically speaking, \bar{F}_{ij} and \bar{F}_{ji} are identical, but to allow for different triangulations on either subdomain [14], we treat them separately.
- \mathcal{F}_i^0 describes the set of indices j for which Ω_i and Ω_j share a face F_{ij} with non-vanishing two-dimensional measure.
- \mathcal{N}_x refers to the set of indexes of subdomains with x in the closure of the subdomain.

Just like in [16], we consider an implicit-explicit (IMEX) time discretization scheme, treating the diffusion term implicitly and the reaction term explicitly. We split the time interval $[0, T]$ into K intervals. With $\tau = t^{k+1} - t^k$, $k = 0, \dots, K$ we derive the following scheme:

$$\begin{aligned} \frac{1}{2} \sum_{i=0}^N \sum_{j \in \mathcal{F}_i^0} \int_{F_{ij}} C_m \frac{[u^{k+1}]_{ij} - [u^k]_{ij}}{\tau} [\phi]_{ij} ds + \sum_{i=0}^N \int_{\Omega_i} \sigma_i \nabla u_i^{k+1} \nabla \phi_i dx \\ = -\frac{1}{2} \sum_{i=0}^N \sum_{j \in \mathcal{F}_i^0} \int_{F_{ij}} F([u^k]_{ij}) [\phi]_{ij} ds. \end{aligned}$$

Rearranging the terms such that we only have $[u^{k+1}]_{ij}$ on the left hand side, we get

$$\begin{aligned} \frac{1}{2} \sum_{i=0}^N \sum_{j \in \mathcal{F}_i^0} \int_{F_{ij}} C_m [u^{k+1}]_{ij} [\phi]_{ij} ds + \tau \sum_{i=0}^N \int_{\Omega_i} \sigma_i \nabla u_i^{k+1} \nabla \phi_i dx \\ = \frac{1}{2} \sum_{i=0}^N \sum_{j \in \mathcal{F}_i^0} \int_{F_{ij}} C_m [u^k]_{ij} [\phi]_{ij} ds - \frac{1}{2} \tau \sum_{i=0}^N \sum_{j \in \mathcal{F}_i^0} \int_{F_{ij}} F([u^k]_{ij}) [\phi]_{ij} ds. \end{aligned} \tag{2}$$

This now lets us define the following local (bi-)linear forms:

$$\begin{aligned}
a_i(u_i, \phi_i) &:= \int_{\Omega_i} \sigma_i \nabla u_i \nabla \phi_i dx, \\
p_i(u_i, \phi_i) &:= \frac{1}{2} \sum_{j \neq i} \int_{F_{ij}} C_m \llbracket u \rrbracket_{ij} \llbracket \phi \rrbracket_{ij} ds, \\
f_i(\phi_i) &:= \frac{1}{2} \sum_{j \neq i} \int_{F_{ij}} (C_m \llbracket u^k \rrbracket_{ij} \llbracket \phi \rrbracket_{ij} - \tau F(\llbracket u^k \rrbracket_{ij}) \llbracket \phi \rrbracket_{ij}) ds, \\
d_i(u_i, \phi_i) &:= \tau a_i(u_i, \phi_i) + p_i(u_i, \phi_i).
\end{aligned} \tag{3}$$

The global problem now reads: Find $u = \{u_i\}_{i=0}^N \in V(\Omega)$ such that

$$d_h(u, \phi) = f(\phi), \quad \forall \phi = \{\phi_i\}_{i=0}^N \in V(\Omega), \tag{4}$$

where $d_h(u, \phi) := \sum_{i=0}^N d_i(u_i, \phi_i) = \sum_{i=0}^N (\tau a_i(u_i, \phi_i) + p_i(u_i, \phi_i))$ and $f(\phi) := \sum_{i=0}^N f_i(\phi_i)$. With local stiffness matrices A_i and mass matrices M_i , (4) corresponding to a_i and p_i , respectively, can be written in matrix form:

$$Ku = f, \quad \text{where } K = \sum_{i=0}^N K_i, \quad K_i = \tau A_i + M_i. \tag{5}$$

3 BDDC and Function Spaces

In this section, we will first construct the function spaces necessary for our preconditioner, extending the theory in [16] to the three-dimensional case. Next, we will construct a family of BDDC preconditioners with different classes of primal constraints, building on results from [12, 13, 14, 16] before concluding the section with some technical tools required for the proof of a condition number bound in the next section.

3.1 Function Spaces

Considering a family of partitionings such that each subdomain is the union of shape-regular conforming finite elements, we define the global interface Γ as the set of points belonging to at least two subdomains:

$$\Gamma := \bigcup_{i=0}^N \Gamma_i, \quad \Gamma_i := \overline{\partial\Omega_i} \setminus \partial\Omega.$$

As in [16], we consider discontinuous Galerkin type discretizations in order to correctly treat jumps of the electric potentials along the cell membrane and gap junctions of each myocyte, which means that the degrees of freedom on the interface Γ will have a multiplicity depending on the number of subdomains that share them.

We further assume that the finite elements are of diameter h and that all subdomains are shape regular with a characteristic diameter H_i . We denote $H = \max_i H_i$.

Considering the multiplicity of degrees of freedom on the interface, we denote with $\Omega'_i = \overline{\Omega}_i \cup \bigcup_{j \in \mathcal{F}_i^0} \overline{F}_{ji}$ the union of nodes in Ω_i and on faces $\overline{F}_{ji} \subset \partial\Omega_j$, $j \in \mathcal{F}_i^0$ and we define the according local finite element spaces

$$W_i(\Omega'_i) := V_i(\overline{\Omega}_i) \times \prod_{j \in \mathcal{F}_i^0} W_i(\overline{F}_{ji}).$$

Here, $W_i(\overline{F}_{ji})$ is the trace of the space $V_j(\overline{\Omega}_j)$ on $F_{ji} \subset \partial\Omega_j$ for all $j \in \mathcal{F}_i^0$. See Figure 2 for a visualization of $W_i(\Omega'_i)$. Each function $u_i \in W_i(\Omega'_i)$ in this space can then be written as

$$u_i = \{(u_i)_i, \{(u_i)_j\}_{j \in \mathcal{F}_i^0}\} \tag{6}$$

where $(u_i)_i$ and $(u_i)_j$ are the restrictions of u_i to $\overline{\Omega}_i$ and \overline{F}_{ji} , respectively.

Again as in [16], we partition $W_i(\Omega'_i)$ into its interior part $W_i(I_i)$ and the finite element trace space $W_i(\Gamma'_i)$, so

$$W_i(\Omega'_i) = W_i(I_i) \times W_i(\Gamma'_i)$$

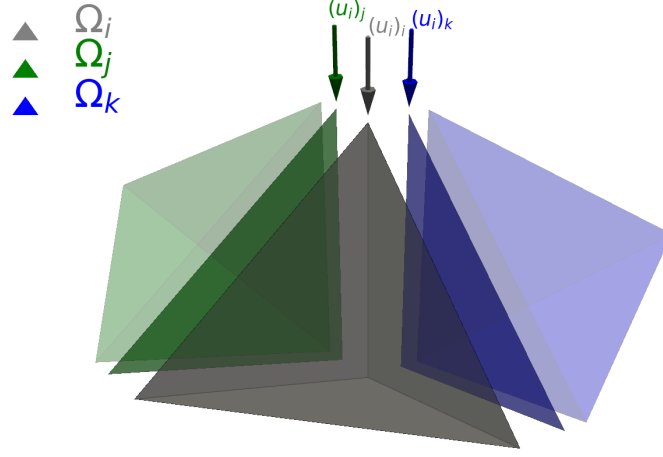


Figure 2: Schematic visualization of the FE space for a tetrahedral substructure Ω_i (grey) with two neighboring substructures. $u_i \in W(\Omega'_i)$ will consist of $(u_i)_i$ on the substructure Ω_i and of $(u_i)_j$ and $(u_i)_k$, the traces of $V_{\{j,k\}}(\Omega_{\{j,k\}})$ on the faces F_{ji} (green) and F_{ki} (blue), respectively.

where $\Gamma'_i = \Gamma_i \cup \{\bigcup_{j \in \mathcal{F}_i^0} \bar{F}_{ji}\}$ denotes the local interface nodes in Ω'_i . This allows a representation of (6) as

$$u_i = (u_{i,I}, u_{i,\Gamma'}), \quad (7)$$

where $u_{i,I}$ represents the values of u_i at the interior nodes on I_i and $u_{i,\Gamma'}$ denotes the values at the nodes on Γ'_i . We consider the product spaces

$$W(\Omega') := \prod_{i=0}^N W_i(\Omega'_i), \quad W(\Gamma') := \prod_{i=0}^N W_i(\Gamma'_i).$$

Here, $u \in W(\Omega')$ means that $u = \{u_i\}_{i=0}^N$ with $u_i \in W_i(\Omega'_i)$ and similarly $u_{\Gamma'} \in W(\Gamma')$ means that $u_{\Gamma'} = \{u_{i,\Gamma'}\}_{i=0}^N$ with $u_{i,\Gamma'} \in W_i(\Gamma'_i)$ where $\Gamma' = \prod_{i=0}^N \Gamma'_i$ denotes the global broken interface.

Subdomain Edges will be denoted by $E_{ijk} := \partial F_{ij} \cap \partial F_{ik}$ for two faces F_{ij} and F_{ik} of Ω_i . Similar to the faces, we will treat the three geometrically identical edges E_{ijk} , E_{jik} and E_{kij} separately and we define $\mathcal{E}_i^0 := \{(j,k) | E_{ijk} \text{ is an edge of } \Omega_i\}$.

Finally we define **Subdomain Vertices** as $\mathcal{V}_i := \{\cup_{(j,k) \in \mathcal{E}_i^0} \partial E_{ijk}\}$ and \mathcal{V}'_i as the union of \mathcal{V}_i with all vertices from other subdomains that Ω_i has a share in. We say that $u = \{u_i\}_{i=0}^N \in W(\Omega')$ is continuous at the corners \mathcal{V}_i if

$$(u_i)_i(x) = (u_j)_i(x) \text{ at all } x \in \mathcal{V}_i \text{ for all } j \in \mathcal{N}_x.$$

Definition 1. The discrete harmonic extension \mathcal{H}'_i in the sense of d_i as defined in (3) is defined as

$$\mathcal{H}'_i : W_i(\Gamma') \rightarrow W_i(\Omega'_i), \quad \begin{cases} d_i(\mathcal{H}'_i u_{i,\Gamma'}, v_i) = 0 & \forall v_i \in W_i(\Omega'_i) \\ \mathcal{H}'_i u_{i,\Gamma'} = (u_i)_i & \text{on } \partial \Omega_i \\ \mathcal{H}'_i u_{i,\Gamma'} = (u_i)_j & \text{on } F_{ji} \subset \partial \Omega_j \\ & \text{and on } E_{j,\varepsilon} \subset \partial \Omega_j. \end{cases}$$

With a notion of faces, edges, and vertices, we can define the function spaces relevant for our preconditioner as in [23, 14]:

Definition 2 (Subspaces $\widetilde{W}(\Omega')$ and $\widetilde{W}(\Gamma')$). We define the space $\widetilde{W}(\Omega')$ as the subspace of functions $u = \{u_i\}_{i=0}^N \in W(\Omega')$ for which the following conditions hold for all $0 \leq i \leq N$:

- u is continuous at all corners \mathcal{V}_i .

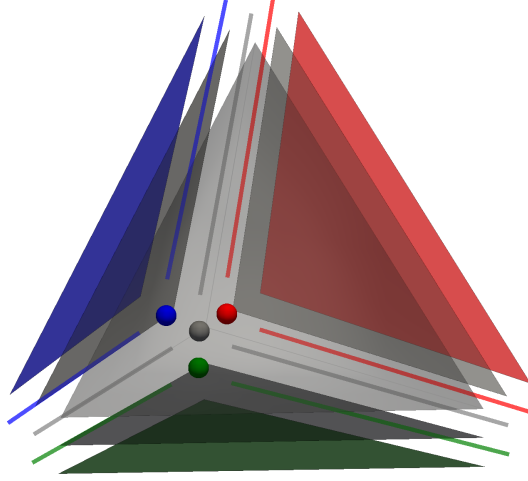


Figure 3: Representation of primal constraints connected to a tetrahedral substructure Ω_i (grey) surrounded by three neighbors (red, green and blue), with the fourth face intersecting with $\partial\Omega$ (the global Neumann boundary). For each face, edge and vertex, one primal constraint per involved substructure is created and on each of them, the according averaging constraints are imposed. In this particular example, Ω_i will contribute to the primal space with 6 face average, 9 edge average and 4 vertex constraints.

- On all edges E_{ijk} for $(j, k) \in \mathcal{E}_i^0$

$$(\bar{u}_i)_{i, E_{ijk}} = (\bar{u}_j)_{i, E_{ijk}} = (\bar{u}_k)_{i, E_{ijk}}.$$

- On all faces F_{ij} for $j \in \mathcal{F}_i^0$

$$(\bar{u}_i)_{i, F_{ij}} = (\bar{u}_j)_{i, F_{ij}}.$$

Here,

$$(\bar{u}_j)_{i, E_{ijk}} = \frac{1}{|E_{ijk}|} \int_{E_{ijk}} (u_j)_i ds, \quad (\bar{u}_j)_{i, F_{ij}} = \frac{1}{|F_{ij}|} \int_{F_{ij}} (u_j)_i ds.$$

We denote with $\widetilde{W}(\Gamma')$ the subspace of $\widetilde{W}(\Omega')$ of functions which are discrete harmonic in the sense of \mathcal{H}'_i .

As indicated in a simplified way by Figure 3, the primal space $\widetilde{W}(\Omega')$ can grow in dimension very quickly, which increases the computational cost of setting up a BDDC preconditioner dramatically, making it desirable to reduce the amount of primal constraints. We therefore also consider the following setting, removing the face averages from the primal space:

Definition 3 (Subspaces $\widetilde{W}_{VE}(\Omega')$ and $\widetilde{W}_{VE}(\Gamma')$). We define the space

$\widetilde{W}_{VE}(\Omega')$ as the subspace of functions $u = \{u_i\}_{i=0}^N \in W(\Omega')$ for which the following conditions hold for all $0 \leq i \leq N$:

- u is continuous at all corners \mathcal{V}_i .
- On all edges E_{ijk} for $(j, k) \in \mathcal{E}_i^0$

$$(\bar{u}_i)_{i, E_{ijk}} = (\bar{u}_j)_{i, E_{ijk}} = (\bar{u}_k)_{i, E_{ijk}}.$$

We define $\widetilde{W}_{VE}(\Gamma')$ in the same way as $\widetilde{W}(\Gamma')$ above.

A function $u \in \widetilde{W}(\Omega')$ (or $u \in \widetilde{W}_{VE}(\Omega')$) can be represented as $u = (u_I, u_\Delta, u_\Pi)$ where $I = \prod_{i=0}^N I_i$ represents the degrees of freedom on interior nodes, Π , which we will call *primal*, denotes degrees of freedom at the vertices \mathcal{V}'_i and

the average face and edge values (or only average edge values in the case of $\widetilde{W}_{VE}(\Omega')$). Δ refers to the remaining nodal degrees of freedom on $\Gamma'_i \setminus \mathcal{V}'_i$ with zero interface averages for the involved interfaces. We will refer to them as *dual*.

Introducing the spaces

$$W_{\Delta}(\Gamma') = \prod_{i=0}^N W_{i,\Delta}(\Gamma'_i) \quad \text{and} \quad \widetilde{W}_{\Pi}(\Gamma')$$

where $W_{i,\Delta}(\Gamma'_i)$ are the local spaces associated with the dual degrees of freedom and $\widetilde{W}_{\Pi}(\Gamma')$ refers to the space associated with the primal degrees of freedom, we can decompose $\widetilde{W}(\Gamma')$ into

$$\widetilde{W}(\Gamma') = W_{\Delta}(\Gamma') \times \widetilde{W}_{\Pi}(\Gamma')$$

and get the representation

$$u_{\Gamma'} \in \widetilde{W}(\Gamma'), \quad u_{\Gamma'} = (u_{\Delta}, u_{\Pi})$$

with $u_{\Pi} \in \widetilde{W}_{\Pi}(\Gamma')$ and $u_{\Delta} = \{u_{i,\Delta}\}_{i=0}^N \in W_{\Delta}(\Gamma')$. Note that we can write $u_{i,\Delta}$ as

$$u_{i,\Delta} = \{ \{u_{i,F_{ij}}, u_{i,F_{ji}}\}_{j \in \mathcal{F}_i^0}, \{u_{i,E_{ijk}}, u_{i,E_{jik}}, u_{i,E_{kij}}\}_{(j,k) \in \mathcal{E}_i^0} \}$$

where $u_{i,F}$ is the restriction of $u_{i,\Delta}$ to the face F , and $u_{i,E}$ is the restriction of $u_{i,\Delta}$ to the edges E . For convenience, Table 1 gives an overview of the above mentioned function spaces.

Space Symbol	Short Description
$V_i(\overline{\Omega}_i)$	local FE space on $\overline{\Omega}_i$
$W_i(\overline{F}_{ji})$	trace of $V_j(\overline{\Omega}_j)$ on the face F_{ji} between subdomains Ω_i and Ω_j
$W_i(\Omega'_i)$	local FE space including duplicated face degrees of freedom
$W_i(I_i)$	interior part of $W_i(\Omega'_i)$
$W_i(\Gamma'_i)$	part of $W_i(\Omega'_i)$ on the broken interface Γ'_i
$W(\Omega'), W(\Gamma')$	global product spaces of the $W_i(\Omega'_i)$ and $W_i(\Gamma'_i)$
$\widetilde{W}(\Omega')$	functions $u \in W(\Omega')$ continuous on vertices with edge and face average constraints
$\widetilde{W}_{VE}(\Omega')$	functions $u \in W(\Omega')$ continuous on vertices with edge but no face average constraints
$\widetilde{W}(\Gamma'), \widetilde{W}_{VE}(\Gamma')$	subspaces of $\widetilde{W}(\Omega')$, $\widetilde{W}_{VE}(\Omega')$ of functions which are discrete harmonic in the sense of \mathcal{H}'_i
$W_{i,\Delta}(\Gamma'_i)$	local space associated with nodal degrees of freedom on $\Gamma'_i \setminus \mathcal{V}'_i$ with zero interface averages for the involved interfaces
$W_{\Delta}(\Gamma')$	global product space of the $W_{i,\Delta}(\Gamma'_i)$
$\widetilde{W}_{\Pi}(\Gamma')$	space of degrees of freedom associated with primal constraints (vertex values and face / edge averages)

Table 1: A list of the function spaces mentioned in Section 3.1 with short descriptions.

3.2 Schur Bilinear Form, Restriction and Scaling Operators

Assuming that in algebraic form, we can write the local problems as $K'_i u_i = f_i$, we can order the degrees of freedom such that the local matrices read

$$K'_i = \begin{bmatrix} K'_{i,II} & K'_{i,I\Gamma'} \\ K'_{i,\Gamma'I} & K'_{i,\Gamma'\Gamma'} \end{bmatrix}. \quad (8)$$

By eliminating the interior degrees of freedom (*static condensation*), our preconditioner will work only on the unknowns on the interface Γ' . In order to do this, we need the local Schur complement systems

$$S'_i := K'_{i,\Gamma'\Gamma'} - K'_{i,\Gamma'}(K'_{i,II})^{-1}K'_{i,I\Gamma'}$$

with which we define the *unassembled* global Schur complement matrix

$$S' = \text{diag}[S'_0, \dots, S'_N].$$

Let $R_{\Gamma'}^{(i)} : W(\Omega') \rightarrow W_i(\Gamma'_i)$ denote the restriction operators returning the local interface components and define $R_{\Gamma'} := \sum_{i=0}^N R_{\Gamma'}^{(i)}$. The global Schur complement matrix is then given by $\widehat{S}_{\Gamma'} = R_{\Gamma'}^T S' R_{\Gamma'}$.

Hence, instead of solving the global linear system $Ku = f$, we can first eliminate the interior degrees of freedom to retrieve a right-hand side $\widehat{f}_{\Gamma'}$ on the interface Γ' , then solve the Schur complement system

$$\widehat{S}_{\Gamma'} u_{\Gamma'} = \widehat{f}_{\Gamma'}$$

and use the solution $u_{\Gamma'}$ on the interface to recover the interior solution as

$$u_{i,I} = (K'_{i,II})^{-1} (f_{i,I} - K'_{i,I\Gamma'} u_{\Gamma'}).$$

The Schur bilinear form can now be defined as

$$d_i(\mathcal{H}'_i u_{i,\Gamma'}, \mathcal{H}'_i v_{i,\Gamma'}) = v_{i,\Gamma'}^T S'_i u_{i,\Gamma'} = s'_i(u_{i,\Gamma'}, v_{i,\Gamma'})$$

and it has the property

$$s'_i(u_{i,\Gamma'}, u_{i,\Gamma'}) = \min_{v_i | \partial\Omega_i \cap \Gamma' = u_{i,\Gamma'}} d_i(v_i, v_i) \quad (9)$$

which allows us to work with discrete harmonic extensions rather than functions only defined on Γ' .

The function spaces from the previous chapter will be equipped with the following restriction operators:

$$\begin{aligned} R_{i,\Delta} : W_{\Delta}(\Gamma') &\rightarrow W_{i,\Delta}(\Gamma'), & R_{\Gamma'\Delta} : W(\Gamma') &\rightarrow W_{\Delta}(\Gamma'), \\ R_{i,\Pi} : \widetilde{W}_{\Pi}(\Gamma') &\rightarrow W_{i,\Pi}(\Gamma'_i), & R_{\Gamma'\Pi} : W(\Gamma') &\rightarrow \widetilde{W}_{\Pi}(\Gamma'). \end{aligned}$$

We further define the direct sums $R_{\Delta} = \oplus R_{i,\Delta}$, $R_{\Pi} = \oplus R_{i,\Pi}$ and $\widetilde{R}_{\Gamma'} = R_{\Gamma'\Pi} \oplus R_{\Gamma'\Delta}$.

For the EMI model, we consider ρ -scaling for the dual variables. For $x \in \overline{\Omega}_i$ it is defined by the pseudoinverses

$$\delta_i^{\dagger}(x) := \frac{\sigma_i}{\sum_{j \in \mathcal{N}_x} \sigma_j}. \quad (10)$$

For $x \notin \overline{\Omega}_i$ we define $\delta_i^{\dagger}(x) = 0$. We note that the δ_i^{\dagger} form a partition of unity, so $\sum_{i=0}^N \delta_i^{\dagger}(x) = 1$ for all $x \in \Omega$.

Recall the following inequality ((6.19) in [23]), it will be an important tool later in this paper:

$$\sigma_i (\delta_j^{\dagger}(x))^2 \leq \min\{\sigma_i, \sigma_j\} \quad \forall j \in \mathcal{N}_x. \quad (11)$$

We define the local scaling operators on each subdomain Ω_i as the diagonal matrix

$$D_i := \text{diag}(\delta_i^{\dagger}), \quad (12)$$

so the i -th scaling matrix contains the coefficients (10) evaluated on the nodal points of Ω_i along the diagonal. With the scaling operators, we can define scaled local restriction operators

$$R_{i,D,\Gamma'} := D_i R_{i,\Gamma'}, \quad R_{i,D,\Delta} := R_{i,\Gamma'\Delta} R_{i,D,\Gamma'},$$

$R_{D,\Delta}$ as the direct sum of the $R_{i,D,\Delta}$ and finally the global scaled restriction operator

$$\widetilde{R}_{D,\Gamma'} := R_{\Gamma'\Pi} \oplus R_{D,\Delta} R_{\Gamma'\Delta}.$$

3.3 The BDDC preconditioner

Introduced in [11], Balancing Domain Decomposition by Constraints (BDDC) is a two-level preconditioner for the Schur complement system $\widehat{S}_{\Gamma'} u_{\Gamma'} = \widehat{f}_{\Gamma'}$. Partitioning the degrees of freedom in each subdomain Ω_i into interior (I), dual (Δ) and primal (Π) degrees of freedom, we can further partition (5) into

$$K'_i = \begin{bmatrix} K'_{i,II} & K'_{i,I\Delta} & K'_{i,I\Pi} \\ K'_{i,\Delta I} & K'_{i,\Delta\Delta} & K'_{i,\Delta\Pi} \\ K'_{i,\Gamma I} & K'_{i,\Gamma\Delta} & K'_{i,\Gamma\Pi} \end{bmatrix}.$$

The action of the BDDC preconditioner is now given by

$$M_{\text{BDDC}}^{-1} x = \widetilde{R}_{D,\Gamma'}^T (\widetilde{S}_{\Gamma'})^{-1} \widetilde{R}_{D,\Gamma'} x, \quad \widetilde{S}_{\Gamma'} = \widetilde{R}_{\Gamma'} S' \widetilde{R}_{\Gamma'}^T,$$

where the inverse of $\tilde{S}_{\Gamma'}^{-1}$ does not have to be computed explicitly but can be evaluated with Block-Cholesky elimination via

$$\tilde{S}_{\Gamma'}^{-1} = \tilde{R}_{\Gamma'\Delta}^T \left(\sum_{i=0}^N \begin{bmatrix} 0 & R_{i,\Delta}^T \\ R_{i,\Delta}^T & \begin{bmatrix} K'_{i,II} & K'_{i,I\Delta} \\ K'_{i,\Delta I} & K'_{i,\Delta\Delta} \end{bmatrix}^{-1} \begin{bmatrix} 0 \\ R_{i,\Delta} \end{bmatrix} \right) \tilde{R}_{\Gamma'\Delta} + \Phi S_{\text{III}}^{-1} \Phi^T.$$

The first term above is the sum of independently computed local solvers on each subdomain Ω'_i , and the second term is a coarse solver for the primal variables (which is computed independently of the local solvers), where

$$\begin{aligned} \Phi &= R_{\Gamma'\Pi}^T - R_{\Gamma'\Delta}^T \sum_{i=0}^N \begin{bmatrix} 0 & R_{i,\Delta}^T \\ R_{i,\Delta}^T & \begin{bmatrix} K'_{i,II} & K'_{i,I\Delta} \\ K'_{i,\Delta I} & K'_{i,\Delta\Delta} \end{bmatrix}^{-1} \begin{bmatrix} K_{i,I\Pi} \\ R_{i,\Delta\Pi} \end{bmatrix} \end{bmatrix} R_{i,\Pi}, \\ S_{\text{III}} &= \sum_{i=0}^N R_{i,\Pi}^T (K'_{i,\Pi\Pi} - \begin{bmatrix} K_{i,\Pi I} & K'_{i,\Pi\Delta} \end{bmatrix} \begin{bmatrix} K'_{i,II} & K'_{i,I\Delta} \\ K'_{i,\Delta I} & K'_{i,\Delta\Delta} \end{bmatrix}^{-1} \begin{bmatrix} K_{i,I\Pi} \\ R_{i,\Delta\Pi} \end{bmatrix}) R_{i,\Pi}. \end{aligned}$$

3.4 Technical Tools and Assumptions

As in [16], we will utilize the following Lemma that is proven considering the continuity and coercivity of the standard Laplacian bilinear form a_i :

Lemma 1. *For the bilinear form $d_i(u_i, v_i) = \tau a_i(u_i, v_i) + p_i(u_i, v_i)$ with a_i and p_i as defined in (3), the following bounds hold:*

$$\begin{aligned} d_i(u_i, u_i) &\leq \tau \sigma_M |u_i|_{H^1(\Omega_i)}^2 + \sum_{j \neq i} \frac{C_m}{2} \|u_i - u_j\|_{L^2(F_{ij})}^2, \\ d_i(u_i, u_i) &\geq \tau \sigma_m |u_i|_{H^1(\Omega_i)}^2 + \sum_{j \neq i} \frac{C_m}{2} \|u_i - u_j\|_{L^2(F_{ij})}^2, \end{aligned}$$

for all $u_i \in V_i(\Omega_i)$ with σ_m and σ_M being the minimum and maximum values of the coefficients σ_i , respectively.

We assume that the cardiac domain $\Omega \subset \mathbb{R}^3$ is subdivided into substructures $\Omega_i \subset \mathbb{R}^3$ which have Lipschitz-continuous boundaries. We will work with Sobolev spaces on subsets $\Lambda \subset \partial\Omega_i$ of the subdomain boundaries which have non-vanishing two-dimensional (faces) or one-dimensional (edges) measure and are relatively open to $\partial\Omega_i$. We will mostly consider the space $H^{1/2}(\Lambda)$ of functions $u \in L^2(\Lambda)$ with finite semi-norm $|u|_{H^{1/2}(\Lambda)} < \infty$ and norm

$$\|u\|_{H^{1/2}(\Lambda)}^2 = \|u\|_{L^2(\Lambda)}^2 + |u|_{H^{1/2}(\Lambda)}^2 < \infty.$$

We will also use the set of functions in $H^{1/2}(\Lambda)$ which extend to zero from Λ to $\partial\Omega_i$ by the extension operator \mathcal{E}_{ext}

$$\mathcal{E}_{\text{ext}} : \Lambda \rightarrow \partial\Omega_i, \quad \mathcal{E}_{\text{ext}} u = \begin{cases} 0 & \text{on } \partial\Omega_i \setminus \Lambda \\ u & \text{on } \Lambda. \end{cases}$$

We will denote this space by

$$H_{00}^{1/2}(\Lambda) = \{u \in H^{1/2}(\Lambda) : \mathcal{E}_{\text{ext}} u \in H^{1/2}(\partial\Omega_i)\}.$$

Remark 1. *For notational convenience, we will write $A \lesssim B$ whenever $A \leq cB$ where c is some constant independent on problem parameters (like e.g. subdomain sizes, mesh size, or conductivity coefficients).*

The following Lemmas will be used in the theoretical analysis in the next chapter, their proofs can be found in [23] (Lemma 4.17, Lemma 4.19 and Lemma 4.26).

Lemma 2. *Let $\bar{u}_{E_{ijk}}$ be the average value of u over E_{ijk} , an edge of the face F_{ij} . Then,*

$$\|u\|_{L^2(E_{ijk})}^2 \lesssim \left(1 + \log \frac{H}{h}\right) \|u\|_{H^{1/2}(F_{ij})}^2$$

and

$$\|u - \bar{u}_{E_{ijk}}\|_{L^2(E_{ijk})}^2 \lesssim \left(1 + \log \frac{H}{h}\right) |u|_{H^{1/2}(F_{ij})}^2.$$

In short, Lemma 2 will enable us to bound edge terms by face terms of an adjacent face. Another inequality we will leverage for the edge terms is

Lemma 3. Let E_{ijk} be an edge of a subdomain Ω_i and let $u \in V^h$. Then,

$$|\mathcal{H}'_i(\Theta_{E_{ijk}}u)|_{H^{1/2}(\partial\Omega_i)}^2 \lesssim \|I^h\Theta_{E_{ijk}}u\|_{L^2(E_{ijk})}^2,$$

where $\Theta_{E_{ijk}}$ is the characteristic finite element function on the edge E_{ijk} and I^h is the usual finite element interpolant.

The following Lemma will be useful for the proof considering reduced primal space only containing vertex and edge average constraints:

Lemma 4. Let $\bar{u}_\mathcal{E}$ be the average of u over \mathcal{E} , an edge of subdomain Ω_i . Let $H_\mathcal{E}$ be the diameter of this edge. Then,

$$(\bar{u}_\mathcal{E})^2 \lesssim \frac{1}{H_\mathcal{E}} \|u\|_{L^2(\mathcal{E})}^2.$$

For face terms, we will use the following inequality:

Lemma 5. Let F_{ij} be a face of a subdomain Ω_i , let $u \in V^h$ and $\bar{u}_{F_{ij}}$ be the average of u over F_{ij} . Then,

$$\|\Theta_{F_{ij}}\|_{H_{00}^{1/2}(F_{ij})} \lesssim \left(1 + \log \frac{H}{h}\right) H$$

and

$$\|I^h\Theta_{F_{ij}}(u - \bar{u}_{F_{ij}})\|_{H_{00}^{1/2}(F_{ij})}^2 \lesssim \left(1 + \log \frac{H}{h}\right)^2 |u|_{H^{1/2}(\partial\Omega_i)}^2.$$

Finally, we will consider the following classical, well-known results throughout the proof. They can be found for example in Appendix A of [23].

Lemma 6. Let $\Lambda \subset \partial\Omega_i$. Then, for $u \in H_{00}^{1/2}$ it holds that

$$\|\mathcal{E}_{ext}u\|_{H^{1/2}(\partial\Omega_i)}^2 \lesssim \|u\|_{H_{00}^{1/2}(\Lambda)}^2 \lesssim \|\mathcal{E}_{ext}u\|_{H^{1/2}(\partial\Omega_i)}^2.$$

Theorem 1 (Trace theorem). Let Ω_i be a polyhedral domain. Then,

$$|u|_{H^{1/2}(\Gamma_i)} \sim |\mathcal{H}_i^\Delta u|_{H^1(\Omega_i)}.$$

4 Bound for the Jump Operator

The main tool in the theory of dual-primal iterative substructuring methods is given by the **jump operator** $P_D : W(\Gamma') \rightarrow W(\Gamma')$, whose action on a given $u \in W(\Gamma')$ is given by $P_D = I - E_D$, where E_D is the averaging operator defined by

$$(E_D u)_i(x) = \left(\sum_{j \in \mathcal{N}_x} \delta_j^\dagger(x) (u_j)_i(x), \left\{ \sum_{j \in \mathcal{N}_x} \delta_j^\dagger(x) (u_j)_{j_0}(x) \right\}_{j_0 \in \mathcal{F}_i^0, j_0 \in (k,l) \in \mathcal{E}_i^0} \right). \quad (13)$$

For this projection, for $x \in \Gamma_i$ it holds that

$$\begin{aligned} ((E_D u)_i)_i(x) &= \sum_{j \in \mathcal{N}_x} \delta_j^\dagger(x) (u_j)_i(x) = ((E_D u)_{j_0})_i(x) \quad \forall j_0 \in \mathcal{N}_x, \\ ((E_D u)_i)_{j_0}(x) &= \sum_{j \in \mathcal{N}_x} \delta_j^\dagger(x) (u_j)_{j_0}(x) = ((E_D u)_{j_0})_{j_0}(x) \quad \forall j_0 \in \mathcal{F}_i^0, j_0 \in (k,l) \in \mathcal{E}_i^0 \end{aligned}$$

and it induces the local action of the jump operator for this particular application as

$$\begin{aligned} (P_D u)_i(x) &= \left(\sum_{j \in \mathcal{N}_x} \delta_j^\dagger(x) ((u_i)_i(x) - (u_j)_i(x)), \right. \\ &\quad \left. \left\{ \sum_{j \in \mathcal{N}_x} \delta_j^\dagger(x) ((u_i)_{j_0}(x) - (u_j)_{j_0}(x)) \right\}_{j_0 \in \mathcal{F}_i^0, j_0 \in (k,l) \in \mathcal{E}_i^0} \right). \end{aligned} \quad (14)$$

The main contribution of this work is a bound on the norm of this operator with respect to the seminorm $|\cdot|_{S'_i}$ induced by the Schur operator:

$$|v|_{S'}^2 := \sum_{i=0}^N |v_i|_{S'_i}^2, \quad |v_i|_{S'_i}^2 := v_i^T S'_i v_i, \quad \text{for } v_i \in W(\Gamma'_i).$$

Lemma 7. *Let the primal space $\widetilde{W}_\Pi(\Gamma')$ be spanned by the vertex nodal degrees finite element functions and the face and edge averages. If the jump operator P_D is scaled by the ρ -scaling as defined in (10), then*

$$|P_D u|_{S'}^2 \leq C \left(1 + \log \frac{H}{h}\right)^2 |u|_{S'}^2 \quad (15)$$

holds for all $u \in \widetilde{W}(\Gamma')$ with C constant and independent of all parameters of the problem. Here, τ is the time step and h the mesh size.

Proof. As in [16], we need only consider the local contributions

$$\begin{aligned} v_i &:= (P_D u)_i \\ &= \left(\sum_{j \in \mathcal{N}_x} I^h \delta_j^\dagger ((u_i)_i - (u_j)_i), \left\{ \sum_{j \in \mathcal{N}_x} I^h \delta_j^\dagger ((u_i)_{j_0} - (u_j)_{j_0}) \right\}_{j_0 \in \mathcal{F}_i^0, j_0 \in (k, l) \in \mathcal{E}_i^0} \right) \\ &= \sum_{\mathcal{F}} I^h(\Theta_{\mathcal{F}} v_i) + \sum_{\mathcal{E}} I^h(\Theta_{\mathcal{E}} v_i) + \sum_{\mathcal{V}} I^h(\Theta_{\mathcal{V}} v_i). \end{aligned}$$

Here $\Theta_* = (\theta_*^i, \theta_*^{j_1}, \dots, \theta_*^{j_k})$ is the characteristic finite element function associated to the faces ($k = 1$), edges ($k = 2$) and vertices ($* \in \{\mathcal{F}, \mathcal{E}, \mathcal{V}\}$) and I^h is the usual finite element interpolant

$$I^h : \mathcal{C}^0(\Omega'_i) \rightarrow W_i(\Omega'_i).$$

Since the vertices are in the primal space, the vertex term vanishes and we have to estimate the contributions given by the faces and edges

$$|v_i|_{S'_i}^2 \lesssim \sum_{\mathcal{F}} |I^h(\Theta_{\mathcal{F}} v_i)|_{S'_i}^2 + \sum_{\mathcal{E}} |I^h(\Theta_{\mathcal{E}} v_i)|_{S'_i}^2.$$

For $* \in \{\mathcal{E}, \mathcal{F}\}$, the ellipticity property of the bilinear form d_i as defined in (3) gives

$$\begin{aligned} |I^h(\Theta_* v_i)|_{S'_i}^2 &= s'_i (I^h(\Theta_* v_i), I^h(\Theta_* v_i)) = d_i(\mathcal{H}'_i I^h(\Theta_* v_i), \mathcal{H}'_i I^h(\Theta_* v_i)) \\ &\leq \tau \sigma_i |\mathcal{H}'_i \Delta I^h(\Theta_* v_i)|_{H^1(\Omega_i)}^2 + \sum_{j \in \mathcal{F}_i^0} \frac{C_m}{2} \|v_i - v_j\|_{L^2(F_{ij})}^2. \end{aligned} \quad (16)$$

For the second term in (16), we use the same argumentation as in [16] to get

$$\|I^h(v_i - v_j)\|_{L^2(F_{ij})} \lesssim |u_i|_{S'_i}^2 + |u_j|_{S'_j}^2. \quad (17)$$

For the first term, we have to distinguish between edge and face terms.

Edge Terms: Consider the edge $\mathcal{E} = E_{ijk}$. We have to consider three terms contributing to

$$\sigma_i |\mathcal{H}'_i \Delta (I^h(\Theta_{E_{ijk}} v_i))|_{H^1(\Omega_i)}^2 \lesssim \sum_{l \in \{i, j, k\}} \sigma_i (\delta_l^\dagger)^2 \|\mathcal{H}'_i \Delta (I^h \Theta_{E_{ijk}} ((u_i)_i - (u_l)_i))\|_{H^1(\Omega_i)}^2. \quad (18)$$

For $l = i$, the term vanishes and for $l \in \{j, k\}$ we get

$$\begin{aligned} &\sigma_i (\delta_l^\dagger)^2 \|\mathcal{H}'_i \Delta (I^h \Theta_{\mathcal{E}} ((u_i)_i - (u_l)_i))\|_{H^1(\Omega_i)}^2 \\ &\lesssim \sigma_i (\delta_l^\dagger)^2 \|I^h \Theta_{\mathcal{E}} ((u_i)_i - (u_l)_i)\|_{H^{1/2}(\partial\Omega_i)}^2 \\ &\lesssim \sigma_i (\delta_l^\dagger)^2 \|I^h(\Theta_{\mathcal{E}}((u_i)_i - (\bar{u}_i)_{i, \mathcal{E}}) - \Theta_{\mathcal{E}}((u_l)_i - (\bar{u}_l)_{i, \mathcal{E}}))\|_{L^2(\mathcal{E})}^2 \\ &\lesssim \sigma_i \|(u_i)_i - (\bar{u}_i)_{i, \mathcal{E}}\|_{L^2(\mathcal{E})}^2 + \sigma_l \|(u_l)_i - (\bar{u}_l)_{i, \mathcal{E}}\|_{L^2(\mathcal{E})}^2 \\ &\lesssim \left(1 + \log \frac{H}{h}\right) \left(\sigma_i \|(u_i)_i\|_{H^{1/2}(F_{il_1})}^2 + \sigma_l \|(u_l)_i\|_{H^{1/2}(F_{ll_2})}^2\right) \\ &\lesssim \left(1 + \log \frac{H}{h}\right) \left(\frac{1}{\tau} |u_i|_{S'_i}^2 + \frac{1}{\tau} |u_j|_{S'_j}^2\right) \end{aligned}$$

where we use Lemma 3, the equal edge averages, (11) and then Lemma 2 for some face F_{il_1} of Ω_i and some face F_{ll_2} of Ω_l .

Summing up, we have shown that

$$|I^h \Theta_{E_{ijk}} v_i|_{S'_i}^2 \lesssim \left(1 + \log \frac{H}{h}\right) \sum_{l \in \{i,j,k\}} |u_l|_{S'_l}^2. \quad (19)$$

Face Terms: In the same way, considering the face $\mathcal{F} = F_{ij}$ between subdomains Ω_i and Ω_j we get

$$\begin{aligned} & \sigma_i |\mathcal{H}_i^\Delta(I^h(\Theta_{F_{ij}} v_i))|_{H^1(\Omega_i)}^2 \\ & \lesssim \sigma_i (\delta_j^\dagger)^2 \|\mathcal{H}_i^\Delta(I^h \Theta_{F_{ij}}((u_i)_i - (u_j)_i))\|_{H^1(\Omega_i)}^2 \\ & \lesssim \sigma_i (\delta_j^\dagger)^2 \|I^h \Theta_{F_{ij}}((u_i)_i - (u_j)_i)\|_{H^{1/2}(\Gamma_i)}^2 \\ & \lesssim \sigma_i (\delta_j^\dagger)^2 \|I^h \Theta_{F_{ij}}((u_i)_i - (u_j)_i)\|_{H_0^{1/2}(F_{ij})}^2 \\ & \lesssim \sigma_i \|I^h \Theta_{F_{ij}}((u_i)_i - (\bar{u}_i)_{i,F_{ij}})\|_{H_0^{1/2}(F_{ij})}^2 + \sigma_j \|I^h \Theta_{F_{ij}}((u_j)_i - (\bar{u}_j)_{i,F_{ij}})\|_{H_0^{1/2}(F_{ij})}^2 \\ & \lesssim \left(1 + \log \frac{H}{h}\right)^2 (\sigma_i |(u_i)_i|_{H^{1/2}(F_{ij})}^2 + \sigma_j |(u_j)_i|_{H^{1/2}(F_{ij})}^2) \\ & \lesssim \left(1 + \log \frac{H}{h}\right)^2 \left(\frac{1}{\tau} |u_i|_{S'_i}^2 + \frac{1}{\tau} |u_j|_{S'_j}^2\right) \end{aligned} \quad (20)$$

where we use (11) and Lemma 5.

Adding up over all substructures, faces and edges, (17), (19) and (20) finally give the inequality

$$|P_D u|_{S'}^2 \lesssim \left(1 + \log \frac{H}{h}\right)^2 |u|_{S'}^2.$$

□

We can show a similar result considering the space \widetilde{W}_{VE} , reaching the same asymptotic behavior with fewer primal constraints:

Lemma 8. *Let the primal space $\widetilde{W}_\Pi(\Gamma')$ be spanned by the vertex nodal degrees finite element functions and the edge averages. If the jump operator P_D is scaled by the ρ -scaling as defined in (10), then*

$$|P_D u|_{S'}^2 \leq C \left(1 + \log \frac{H}{h}\right)^2 |u|_{S'}^2, \quad (21)$$

holds for all $u \in \widetilde{W}_{VE}(\Gamma')$ with C constant and independent of all parameters of the problem.

Proof. We proceed just as in the proof of Lemma 7 for edge terms. For face terms, the averages $(\bar{u}_i)_{i,F_{ij}}$ and $(\bar{u}_j)_{i,F_{ij}}$ will now generally be different. Therefore, following the argumentation of Lemma 6.36 in [23] we reach that

$$\begin{aligned} & \sigma_i (\delta_j^\dagger)^2 \|I^h \Theta_{F_{ij}}((u_i)_i - (u_j)_i)\|_{H_0^{1/2}(F_{ij})}^2 \\ & = \sigma_i (\delta_j^\dagger)^2 \|I^h \Theta_{F_{ij}}(((u_i)_i - (\bar{u}_i)_{i,F_{ij}}) - ((u_j)_i - (\bar{u}_j)_{i,F_{ij}})) \\ & \quad + ((\bar{u}_i)_{i,F_{ij}} - (\bar{u}_j)_{i,F_{ij}}))\|_{H_0^{1/2}(F_{ij})}^2 \\ & \lesssim \sigma_i \|I^h \Theta_{F_{ij}}((u_i)_i - (\bar{u}_i)_{i,F_{ij}})\|_{H_0^{1/2}(F_{ij})}^2 + \sigma_j \|I^h \Theta_{F_{ij}}((u_j)_i - (\bar{u}_j)_{i,F_{ij}})\|_{H_0^{1/2}(F_{ij})}^2 \\ & \quad + \min\{\sigma_i, \sigma_j\} \|\Theta_{F_{ij}}((\bar{u}_i)_{i,F_{ij}} - (\bar{u}_j)_{i,F_{ij}})\|_{H_0^{1/2}(F_{ij})}^2. \end{aligned} \quad (22)$$

The first two terms we can estimate exactly as in 20 by

$$(\sigma_i |(u_i)_i|_{H^{1/2}(F_{ij})}^2 + \sigma_j |(u_j)_i|_{H^{1/2}(F_{ij})}^2).$$

We still have to estimate the third term, $\|\Theta_{F_{ij}}((\bar{u}_i)_{i,F_{ij}} - (\bar{u}_j)_{i,F_{ij}})\|_{H_0^{1/2}(F_{ij})}^2$. Since all edge averages are primal, we choose an edge \mathcal{E} of the face F_{ij} and have $(\bar{u}_i)_{i,\mathcal{E}} = (\bar{u}_j)_{i,\mathcal{E}}$. This gives

$$|((\bar{u}_i)_{i,F_{ij}} - (\bar{u}_j)_{i,F_{ij}})|^2 \lesssim |((\bar{u}_i)_{i,F_{ij}} - (\bar{u}_i)_{i,\mathcal{E}})|^2 + |((\bar{u}_j)_{i,F_{ij}} - (\bar{u}_j)_{i,\mathcal{E}})|^2.$$

We only consider the first term and proceed in exactly the same way for the second. Utilizing Lemma 4, we get

$$|((\bar{u}_i)_{i,F_{ij}} - (\bar{u}_i)_{i,\mathcal{E}})|^2 = |(\overline{(\bar{u}_i)_{i,F_{ij}} - (u_i)_i})_{i,\mathcal{E}}|^2 \lesssim \frac{1}{H} \|(\bar{u}_i)_{i,F_{ij}} - (u_i)_i\|_{L^2(\mathcal{E})}^2,$$

and Lemma 2 and Lemma A.17 from [23] now yield

$$|((\bar{u}_i)_{i,F_{ij}} - (\bar{u}_i)_{i,\mathcal{E}})|^2 \lesssim \frac{1}{H} \left(1 + \log \frac{H}{h}\right) |(\bar{u}_i)_{i,F_{ij}} - (u_i)_i|_{H^{1/2}(F_{ij})}^2. \quad (23)$$

Combining (23) with Lemma 5 it finally follows that

$$\|\Theta_{F_{ij}}((\bar{u}_i)_{i,F_{ij}} - (\bar{u}_j)_{i,F_{ij}})\|_{H_0^{1/2}(F_{ij})}^2 \lesssim \left(1 + \log \frac{H}{h}\right)^2 (|(u_i)_i|_{H^{1/2}(F_{ij})}^2 + |(u_j)_i|_{H^{1/2}(F_{ij})}^2)$$

and we can combine the partial results and follow the rest of the argumentation in the proof of Lemma 7. \square

With these results, we finally receive the following condition number bounds for the BDDC-preconditioned linear systems which can be proven as in [23]:

Theorem 2. *Let M^{-1} be the BDDC preconditioner generated as stated above and K the according linear system. Then the condition number $\kappa(M^{-1}K) = \frac{\lambda_{\max}}{\lambda_{\min}}$ is bounded by*

$$\kappa(M^{-1}K) \leq C \left(1 + \log \frac{H}{h}\right)^2,$$

where λ_{\max} and λ_{\min} are the maximum and minimum Eigenvalues of $M^{-1}K$ and C is a constant independent of h , H , and the values of σ_i . This bound holds both if we choose the primal constraints as in Lemma 7 and as in Lemma 8.

5 Numerical Study

We complement the theoretical analysis with experiments. For this, we consider an artificial, repetitive geometry that splits a cube into two subdomains, an intracellular subdomain in the center with connections to the outside via all faces of the cubes and an extracellular domain around it (see Figure 4). This way, each intracellular subdomain has both an interface to an extracellular subdomain (via a cell membrane) and to other intracellular subdomains (via gap junctions). For this study, we consider a linear gap junction for the interfaces between intracellular subdomains and the Aliev-Panfilov ionic model [2] for the gating variables between intra- and extracellular subdomains. If not stated otherwise, the conductivity coefficients σ_i are fixed to $3 \frac{\text{mS}}{\text{cm}}$ for intra- and $20 \frac{\text{mS}}{\text{cm}}$ for extra-cellular subdomains. To improve load balancing, we decompose the extracellular domain into subdomains using regular continuous finite elements. On the interfaces between those subdomains, we do not need to consider any discontinuities. We use the BDDC implementation in the software library Ginkgo [4] as a preconditioner for a Conjugate Gradient (CG) method. The stopping criterion evaluates the L^2 -norm of the residual against a pre-set threshold. All tests have been performed on the CPU partition of the EuroHPC machine Karolina¹ on compute nodes with two AMD Zen 2 EPYC™ 7H12 CPUs, totalling 128 CPU cores and 256 GB of main memory per node.

5.1 Scalability

For a weak scaling study, we consider the linear system in an EMI model simulation at the same time step (0.01 ms) for a growing number of subdomains, starting with $3 \times 3 \times 1$ cells and reaching up to $7 \times 7 \times 7$ cells. The observed convergence behavior aligns with the theory: as we increase the number of subdomains but leave $\frac{H}{h}$ constant, the number of iterations needed to converge as well as the condition number estimate remain roughly constant, see Table 2.

To evaluate the stability of the method, we consider a setup where we run the solver with random right-hand-side vectors. For this study, we generate 100 different right-hand-side vectors filled with random values in $(-1, 1)$ for each of the test cases and record the iteration count needed to converge to a relative residual norm tolerance of 10^{-6} . Figure 5 confirms the expectation that the choice of right-hand side does not impact the convergence of our method significantly. In terms of compute time, we see two major jumps: the first when inter-node communication over the network is needed starting at 128 subdomains, and the second when the solution of the coarse problem starts dominating the runtime. The latter effect can possibly be alleviated by employing a second level of BDDC on the coarse problem to improve scalability.

¹<https://www.it4i.cz/en/infrastructure/karolina>

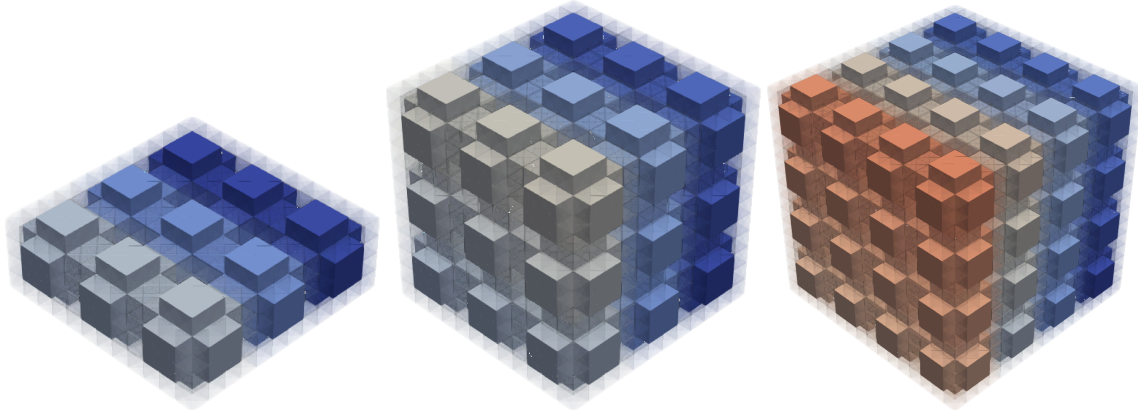


Figure 4: Repetitive test geometry with $3 \times 3 \times 1$ (left), $3 \times 3 \times 3$ (middle) and $4 \times 4 \times 4$ (right) cells. Each cell is an intracellular subdomain inside a cube that can be stacked in all dimensions, resulting in a mesh where all intracellular subdomains have interfaces with extracellular space via a cell membrane model and with other intracellular domains via a linear gap junction.

#cells	#SD	GD	VEF				VE			
			it	κ	CD	time	it	κ	CD	time
$3 \times 3 \times 1$	18	4493	7	2.3158	73	2.9	14	17.4721	40	2.5
$3 \times 3 \times 2$	36	8718	7	2.2712	207	3.3	16	12.2331	123	2.8
$3 \times 3 \times 3$	54	12943	7	2.2587	341	3.8	15	11.9005	206	3.3
$4 \times 4 \times 4$	128	30209	7	2.2605	919	5.4	15	11.7062	567	6
$5 \times 5 \times 5$	250	58461	7	2.2602	1929	5.8	15	11.3865	1204	6.2
$6 \times 6 \times 6$	432	100405	7	2.2602	3491	9.1	15	11.6549	2195	6.6
$7 \times 7 \times 7$	686	158747	7	2.2602	5725	15.6	15	11.6975	3618	15.5

Table 2: Weak scalability for an increasing number of cells from $3 \times 3 \times 1$ to $7 \times 7 \times 7$. Each intra- and extracellular subdomain is discretized with 512 tetrahedral finite elements. We report the number of subdomains (SD), the global dimension (GD) of the linear problem, the number of preconditioner CG iterations (it), a condition number estimate (κ) computed with the Lanczos estimate, the dimension of the coarse problem (CD), and the time needed for a preconditioner application in ms. The stopping criterion tolerance for this test is a residual norm of 10^{-8} .

5.2 Robustness w.r.t. conductivity coefficients

The theoretical results obtained in Section 4 reveal that the condition number of the preconditioned operator is bounded independently of the conductivity coefficients σ_i . In order to evaluate this experimentally, we show in Figure 6 the convergence behavior for random conductivity coefficients in the extracellular and intracellular subdomains. As the extracellular subdomains together represent one continuous space, we assign the same coefficient to all of them, while each of the intracellular subdomains is assigned a random conductivity coefficient. One can observe the same behavior as for fixed σ_i with a slightly wider range of needed iterations.

5.3 Optimality tests

In this section, we evaluate the poly-logarithmic convergence behavior of the preconditioned linear operator. For this, we refine a mesh of $3 \times 3 \times 3$ cells in order to increase the value of $\frac{H}{h}$. In each refinement level, the number of degrees of freedom doubles in each dimension, so $\frac{H}{h}$ also increases by a factor of 2. Figure 7 reveals that the iteration count increases as expected. From the theoretical results, we expect the condition number to grow asymptotically with $(1 + \log \frac{H}{h})^2$ (dashed blue line).

The estimated condition number growth aligns with this expectation. For the reduced coarse space only consisting of edge and vertex constraints, the condition number growth aligns more with linear growth (red dotted line), while flattening out with increasing refinement level.

As our repetitive mesh is constructed out of cells with a potentially problematic geometry (they are not convex), we simplify the geometry to the meshes shown in Figure 8. This way, we intend to observe the asymptotic behavior of the condition number also for the reduced coarse space in Figure 9. We note that while the estimated condition number

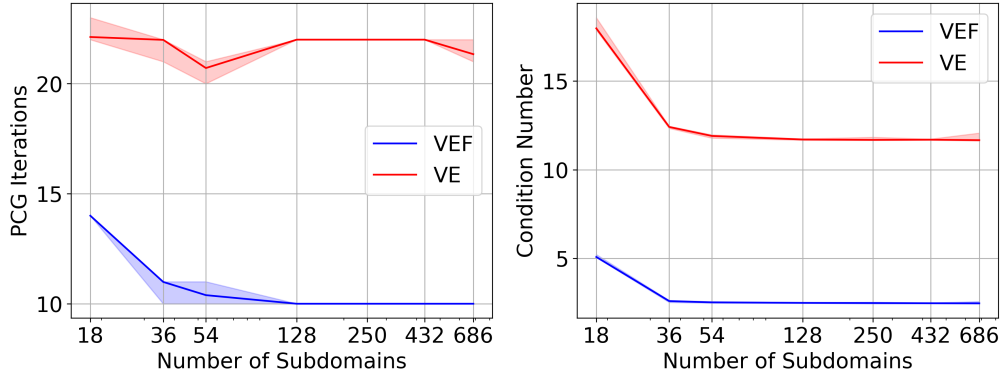


Figure 5: Iterations needed to converge to a relative residual tolerance of 10^{-6} (left) and condition number estimates (right) for random right-hand side vectors. The results colored in blue consider a full primal space containing vertex values as well as edge and face averages. The results colored in red consider only vertex values and edge averages in the primal space. The solid lines show the mean over 100 different random right-hand sides, the colored areas represent the range of iterations or condition numbers for each test case, respectively.

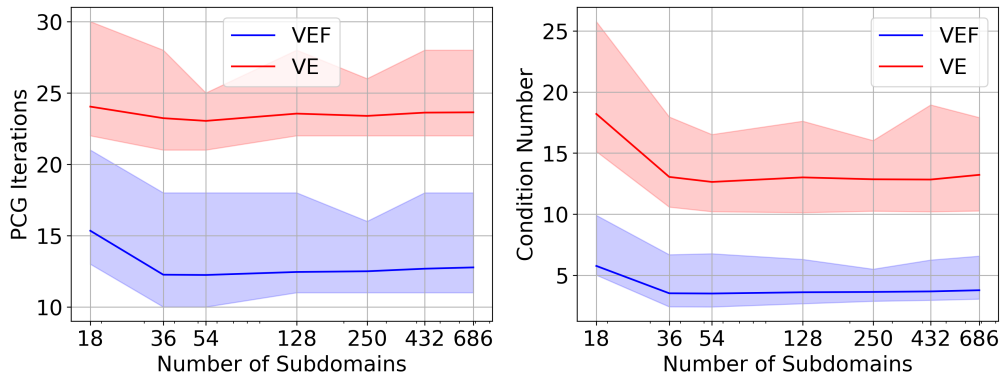


Figure 6: Iterations needed to converge to a relative residual tolerance of 10^{-6} (left) and condition number estimates (right) for random conductivity coefficients $\sigma_i \in (1, 20) \frac{\text{mS}}{\text{cm}}$. For each test case, we generate the preconditioner 100 times with different, random conductivity coefficients, the solid lines show the mean of the iterations needed to converge and the condition number estimates.

of the preconditioned operator reflects the theoretical asymptotic bounds perfectly for the full coarse space and for the reduced coarse space, this is only obvious for the simplest mesh. The actual convergence behavior by iterations reflects poly-logarithmic growth in all cases.

6 Conclusion

In this paper, we have constructed and analyzed the Balancing Domain Decomposition by Constraint preconditioner for composite DG-type discretizations of cardiac cell-by-cell models in three spatial dimensions. We have derived theoretical convergence results and used an experimental evaluation to confirm these bounds for a synthetic test case with a repetitive geometry. We also demonstrated the scalability and quasi-optimality of the preconditioner and the convergence being independent of conductivity coefficients. Future research will include the integration of the method into large-scale cardiac simulations, moving further away from the regularly shaped geometries considered by the theory and towards more organically, irregularly shaped myocytes as they would appear in the human heart.

7 Acknowledgements

This work was supported by the European High-Performance Computing Joint Undertaking EuroHPC under grant agreement No 955495 (MICROCARD) co-funded by the Horizon 2020 programme of the European Union (EU), the

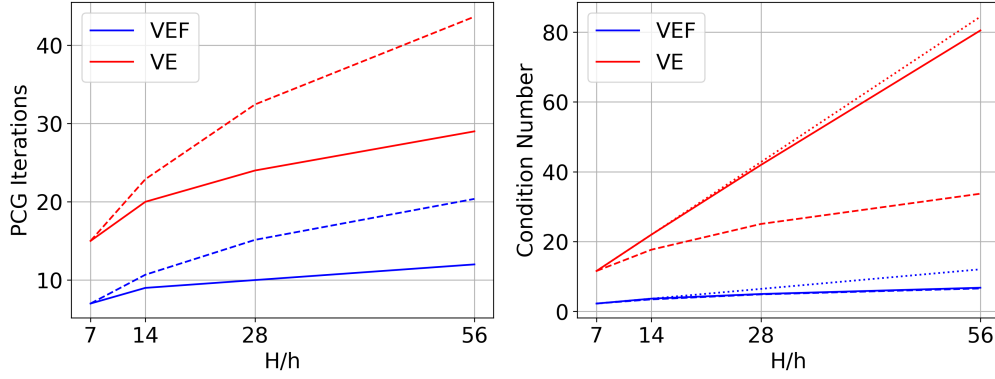


Figure 7: Iterations needed to converge to a relative residual tolerance of 10^{-6} (left) and condition number estimates (right) for an increasing refinement level. Refining the problem increases $\frac{H}{h}$, resulting in poly-logarithmic increase in the condition number and in the iteration count (dashed lines). For the coarse space containing only vertex and edge constraints, the actual growth of the condition number appears to be closer to linear (dotted line). Here, the dashed line is the graph of $\left(1 + \log \frac{H}{h}\right)^2$ scaled such that it intersects with the first measured data point and the dotted line is a linear interpolation of the first two measured data points.

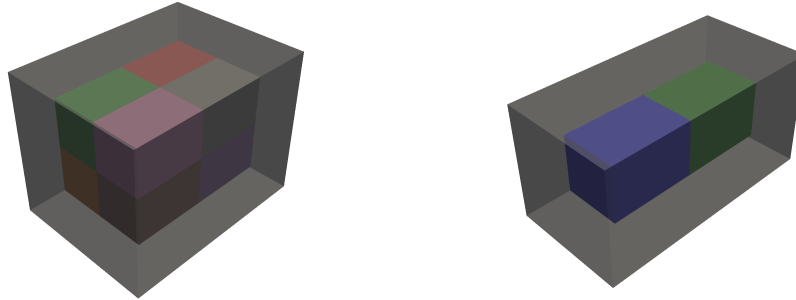


Figure 8: Simplified meshes containing 8 (left) and 2 (right) convex myocytes floating in extracellular space.

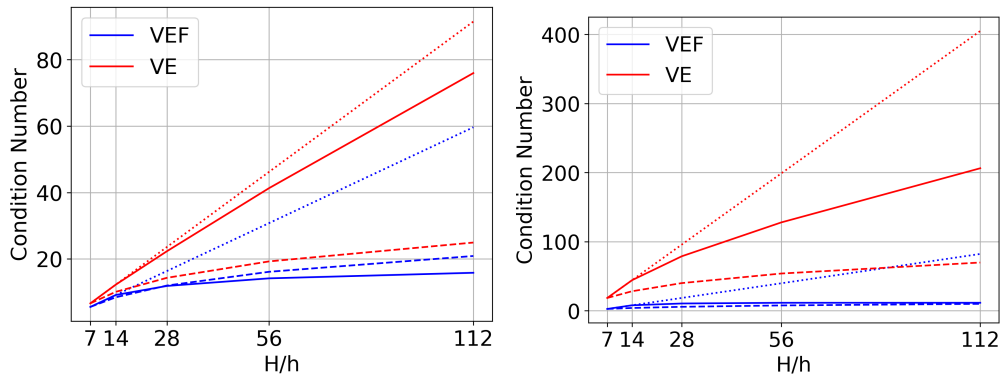


Figure 9: Condition number estimates for increasing refinement levels of simple geometries as shown in Figure 8. For the mesh made up from 8 cells (left), we already see a stronger sub-linear trend than for our repetitive test geometry while for the simplest case containing only two convex cells (right), the behavior shows a poly-logarithmic trend, aligning with the theoretical results. We note that for the simplest geometry, the condition number estimates are generally higher than for the more complex geometries, which is most likely due to the complete lack of primal (vertex) constraints.

French National Research Agency ANR, the German Federal Ministry of Education and Research, the Italian ministry of economic development, the Swiss State Secretariat for Education, Research and Innovation, the Austrian Research Promotion Agency FFG, and the Research Council of Norway.

This work was supported by the MICROCARD-2 project (project ID 101172576). The project is supported by the EuroHPC Joint Undertaking and its members (including top-up funding by ANR, BMBF, and Ministero dello sviluppo economico). Funded by the European Union. Views and opinions expressed are however those of the author(s) only and do not necessarily reflect those of the European Union or EuroHPC. Neither the European Union nor EuroHPC can be held responsible for them.

The authors acknowledge the EuroHPC award for the availability of high-performance computing resources on Karolina (EU2024D09-042). N.M.M.H., L.F.P. and S.S. have been supported by grants of Istituto Nazionale di Alta Matematica (INDAM-GNCS) and by MUR (PRIN 202232A8AN_002, PRIN 202232A8AN_003, PRIN P2022B38NR_001 and PRIN P2022B38NR_002) funded by European Union - Next Generation EU.

References

- [1] *Numerical modeling of cardiac electrophysiology at the cellular scale*, 2021, <https://cordis.europa.eu/project/id/955495>.
- [2] R. R. ALIEV AND A. V. PANFILOV, *A simple two-variable model of cardiac excitation*, *Chaos, Solitons & Fractals*, 7 (1996), pp. 293–301, [https://doi.org/10.1016/0960-0779\(95\)00089-5](https://doi.org/10.1016/0960-0779(95)00089-5).
- [3] P. F. ANTONIETTI AND B. AYUSO, *Schwarz domain decomposition preconditioners for discontinuous galerkin approximations of elliptic problems: non-overlapping case*, *ESAIM: Mathematical Modelling and Numerical Analysis*, 41 (2007), pp. 21–54.
- [4] H. ANZT, T. COJEAN, G. FLEGAR, F. GÖBEL, T. GRÜTZMACHER, P. NAYAK, T. RIBIZEL, Y. M. TSAI, AND E. S. QUINTANA-ORTÍ, *Ginkgo: A Modern Linear Operator Algebra Framework for High Performance Computing*, *ACM Trans. Math. Softw.*, 48 (2022), pp. 2:1–2:33, <https://doi.org/10.1145/3480935>.
- [5] B. AYUSO DE DIOS, M. HOLST, Y. ZHU, AND L. ZIKATANOV, *Multilevel preconditioners for discontinuous galerkin approximations of elliptic problems with jump coefficients*, *Mathematics of Computation*, 83 (2014), pp. 1083–1120.
- [6] P.-E. BÉCUE, M. POTSE, AND Y. COUDIÈRE, *A three-dimensional computational model of action potential propagation through a network of individual cells*, in 2017 Computing in Cardiology (CinC), IEEE, 2017, pp. 1–4.
- [7] P. BENEDUSI, P. FERRARI, M. E. ROGNES, AND S. SERRA-CAPIZZANO, *Modeling excitable cells with the emi equations: spectral analysis and iterative solution strategy*, *Journal of Scientific Computing*, 98 (2024), p. 58.
- [8] A. BUDIŠA, X. HU, M. KUČHTA, K.-A. MARDAL, AND L. ZIKATANOV, *Algebraic multigrid methods for metric-perturbed coupled problems*, *SIAM Journal on Scientific Computing*, 46 (2024), pp. A1461–A1486.
- [9] F. CHEGINI, A. FROHELY, N. HUYNH, L. PAVARINO, M. POTSE, S. SCACCHI, AND M. WEISER, *Efficient numerical methods for simulating cardiac electrophysiology with cellular resolution*, in X International Conference on Computational Methods for Coupled Problems in Science and Engineering COUPLED PROBLEMS 2023, 2023.
- [10] G. R. DE SOUZA, R. KRAUSE, AND S. PEZZUTO, *Boundary integral formulation of the cell-by-cell model of cardiac electrophysiology*, *Engineering Analysis with Boundary Elements*, 158 (2024), pp. 239–251.
- [11] C. R. DOHRMANN, *A Preconditioner for Substructuring Based on Constrained Energy Minimization*, *SIAM Journal on Scientific Computing*, 25 (2003), pp. 246–258, <https://doi.org/10.1137/S1064827502412887>.
- [12] M. DRYJA, J. GALVIS, AND M. SARKIS, *A FETI-DP Preconditioner for a Composite Finite Element and Discontinuous Galerkin Method*, *SIAM Journal on Numerical Analysis*, 51 (2013), pp. 400–422, <https://doi.org/10.1137/100796571>.
- [13] M. DRYJA, J. GALVIS, AND M. SARKIS, *A Deluxe FETI-DP Preconditioner for a Composite Finite Element and DG Method*, *Computational Methods in Applied Mathematics*, 15 (2015), pp. 465–482, <https://doi.org/10.1515/cmam-2015-0025>.
- [14] M. DRYJA AND M. SARKIS, *3-D FETI-DP Preconditioners for Composite Finite Element-Discontinuous Galerkin Methods*, in Domain Decomposition Methods in Science and Engineering XXI, J. Erhel, M. J. Gander, L. Halpern, G. Pichot, T. Sassi, and O. Widlund, eds., Cham, 2014, Springer International Publishing, pp. 127–140, https://doi.org/10.1007/978-3-319-05789-7_10.

- [15] K. HORGMO JÆGER AND A. TVEITO, *Re-Introducing the Cell: The Extracellular-Membrane-Intracellular (EMI) Model*, in *Differential Equations for Studies in Computational Electrophysiology*, K. Horgmo Jæger and A. Tveito, eds., Springer Nature Switzerland, Cham, 2023, pp. 107–117, https://doi.org/10.1007/978-3-031-30852-9_11.
- [16] N. HUYNH, F. CHEGINI, L. PAVARINO, M. WEISER, AND S. SCACCHI, *Convergence analysis of BDDC preconditioners for composite DG discretizations of the cardiac cell-by-cell model*, *SIAM J. Sci. Comput.*, 45(6) (2023), pp. A2836–A2857, <https://doi.org/10.1137/22M1542532>.
- [17] N. M. M. HUYNH, L. F. PAVARINO, AND S. SCACCHI, *Gdsw preconditioners for composite discontinuous galerkin discretizations of multicompartement reaction–diffusion problems*, *Computer Methods in Applied Mechanics and Engineering*, 433 (2025), p. 117501, <https://doi.org/https://doi.org/10.1016/j.cma.2024.117501>, <https://www.sciencedirect.com/science/article/pii/S0045782524007552>.
- [18] K. H. JÆGER, A. G. EDWARDS, W. R. GILES, AND A. TVEITO, *From Millimeters to Micrometers; Re-introducing Myocytes in Models of Cardiac Electrophysiology*, *Frontiers in Physiology*, 12 (2021), p. 763584, <https://doi.org/10.3389/fphys.2021.763584>.
- [19] K. H. JÆGER, K. G. HUSTAD, X. CAI, AND A. TVEITO, *Efficient Numerical Solution of the EMI Model Representing the Extracellular Space (E), Cell Membrane (M) and Intracellular Space (I) of a Collection of Cardiac Cells*, *Frontiers in Physics*, 8 (2021), <https://doi.org/10.3389/fphy.2020.579461>.
- [20] C. PECHSTEIN AND C. R. DOHRMANN, *A unified framework for adaptive bddc*, *Electron. Trans. Numer. Anal.*, 46 (2017), p. 3.
- [21] M. POTSE, B. DUBE, J. RICHER, A. VINET, AND R. M. GULRAJANI, *A comparison of monodomain and bidomain reaction-diffusion models for action potential propagation in the human heart*, *IEEE Transactions on Biomedical Engineering*, 53 (2006), pp. 2425–2435, <https://doi.org/10.1109/TBME.2006.880875>.
- [22] S. ROHR, *Role of gap junctions in the propagation of the cardiac action potential*, *Cardiovascular Research*, 62 (2004), pp. 309–322, <https://doi.org/10.1016/j.cardiores.2003.11.035>.
- [23] A. TOSELLI AND O. B. WIDLUND, *Domain Decomposition Methods–Algorithms and Theory*, no. 34 in *Springer Series in Computational Mathematics*, Springer, Berlin, 2005.
- [24] L. TUNG, *A bi-domain model for describing ischemic myocardial D-C currents*, (2005).
- [25] A. TVEITO, K. H. JÆGER, M. KUCHTA, K.-A. MARDAL, AND M. E. ROGNES, *A Cell-Based Framework for Numerical Modeling of Electrical Conduction in Cardiac Tissue*, *Frontiers in Physics*, 5 (2017), <https://doi.org/10.3389/fphy.2017.00048>.
- [26] A. TVEITO, K.-A. MARDAL, AND M. E. ROGNES, eds., *Modeling Excitable Tissue: The EMI Framework*, Springer Nature, 2021, <https://doi.org/10.1007/978-3-030-61157-6>.
- [27] M. VENERONI, *Reaction–diffusion systems for the microscopic cellular model of the cardiac electric field*, *Mathematical methods in the applied sciences*, 29 (2006), pp. 1631–1661.
- [28] M. VENERONI, *Reaction–diffusion systems for the macroscopic bidomain model of the cardiac electric field*, *Nonlinear Analysis: Real World Applications*, 10 (2009), pp. 849–868, <https://doi.org/10.1016/j.nonrwa.2007.11.008>.